Microscopic Aspects of the Growth of Metastable fcc Iron on the Au(111) Surface

Joseph A. Stroscio, D. T. Pierce and R. A. Dragoset

National Institute of Standards and Technology
Gaithersburg, Maryland 20899

1991 PACS: 61.16.Di, 68.55.Bd, 81.10.Bk

Abstract

We report on the microscopic aspects of the growth of Fe on the Au(111) surface observed with scanning tunneling microscopy. Nucleation of triangular Fe islands is observed to occur at the corners of the herringbone reconstruction of the Au(111) surface. Atomic resolution measurements show the existence of a new metastable close-packed fcc phase of Fe with a 0.288 ±0.01 nm in-plane nearest neighbor distance. Initial fcc film growth proceeds in a layer-by-layer growth mode.

June 3, 1991

Considerable interest exists in the physical properties of ultra-thin metal films. Particularly in magnetic systems this interest has resulted from novel magnetic behavior predicted and observed in the few monolayer (ML) regime.[1] In analogy to band-gap engineering in strained layer epitaxy in semiconductors, one can exploit the dependence of the exchange energy on lattice expansion in epitaxial metal films to produce *new magnetic phases* not found to occur naturally. Such atomic engineering of low dimensional magnetic systems has only recently been realized.[2] Understanding the microscopic aspects of film growth in the submonolayer and ultra-thin film limits is necessary to understand macroscopic measurements of these unique systems, such as magnetoresistance or magneto-optic Kerr effect, and how these correlate with the physical microstructure. Scanning tunneling microscopy (STM) can provide such information as well as a detailed picture of the growth process itself. Recently, it has been shown that the Au(111) surface provides a unique substrate to examine microscopic aspects of metal film growth due to the presence of the long range Au(111) surface reconstruction.[3,4] Silver is known to nucleate at the step edges;[3] whereas the transition metals Ni[4] and, as shown in this work, Fe are observed to nucleate at the herringbone corners.

In this paper we report on the microscopic aspects of the growth of Fe on the Au(111) surface at submonolayer and few monolayer coverages, determined by scanning tunneling microscopy (STM).[5] Islands of Fe are observed to nucleate and grow at the corners of the Au(111) herringbone reconstruction due to a surface lattice dislocation. Atomic resolution images show that these monolayer high islands consist of a new metastable phase of fcc Fe, which is stabilized by the underlying Au(111) surface lattice and expanded by 12% compared to the high temperature fcc γ-Fe phase. With increasing coverage the Fe islands at the nucleation sites increase in size and eventually grow together. The growth approximates layer-by-layer, or Frank-van der Merwe type growth for the first few monolayers. The growth is not the ideal case in which only one layer grows at a time; rather the formation of new layers starts before the preceding layers are complete. For

coverages greater than 3-4 ML, a transition to the bcc structure is inferred from the growth of rectangular Fe islands coincident with a splitting observed in the reflection high energy electron diffraction (RHEED) pattern. The STM data provide a direct visualization of the growth front and thus a means to test theories of epitaxial growth of metal films.[6,7]

The experiments were carried out in an ultra-high vacuum system operating at a pressure < 10^{-10} Torr. The Au(111) crystal was cleaned by Ne ion bombardment while annealing the crystal at 500 °C. Fe was evaporated with the sample at room temperature at a rate of 0.2-0.5 ML/min using two different sources: one using *e*-beam heating and another using a thermal W filament wound with Fe, yielding identical results. Fe coverages were determined from the STM images. The STM measurements were obtained on a newly built instrument capable of resolving corrugations at the picometer level, which facilitated atomic resolution measurements on metal surfaces. Single crystal (111) oriented W wire was used for probe tips, which all displayed 3-fold symmetric field emission patterns prior to STM measurements.

The initial nucleation of Fe islands of about 1-2 nm in diameter at the corners of the herringbone reconstruction of the Au(111) surface is shown in Fig. 1. The superlattice of the reconstruction causes Fe to nucleate in an ordered array of islands with a spacing of ~12.5 nm between rows of islands running along the [$1\bar{2}1$] direction (see arrows in Fig. 1) and ~7.3 nm between islands in these rows. The preferential nucleation results from the structural imperfections at the bulged corners of the Au(111) herringbone reconstruction. This reconstruction consists of partial dislocation ridges resulting from the uniaxial 4.2% contraction along the <$1\bar{1}0$> directions, where there are 23 atoms for every 22 sites resulting in a $23x\sqrt{3}$ unit cell.[3,8] These ridges result from atoms in bridge sites (at elevated positions) and separate regions where atoms are in the hollow sites of fcc (ABC) and hcp (ABA) stacking. The double ridges are periodic with a period of 6.3 nm; the larger spacing between individual ridges corresponds to regions of fcc stacking (more energetically favored) while the narrower regions correspond to hcp stacking (see Fig. 2). On large

enough terraces the reconstruction forms a superstructure where the ridges lie along the $<11\bar{2}>$ directions, meeting at 120^{o} angles.

Atomic resolution images of one of the bulging corners in the herringbone reconstruction are shown in Fig. 2. Note that the corrugation in the image is 3 pm (0.003 nm) measured with a gap resistance of about 10^{9} ohms, which is routinely obtained. A few picometers corrugation corresponds to normal charge density profiles expected in the Tersoff-Hamann tunneling theory,[9] in contrast to anomalous corrugations obtained with tunneling gaps approaching point contact.[8] This capability allows us to perform atomic resolution imaging of metals without strong tip-surface interactions, which may interfere with the object being measured.

Fig. 2(a) shows the shift in the atomic rows in going through the transition region from fcc to hcp stacking in the Au(111) reconstruction; the line initially is lined up on a column of atoms in the fcc region and ends up between two columns in the hcp region. A close up of the corner in the herringbone is shown in Fig. 2(b).The lines highlight the $[0\bar{1}1]$ atomic rows in the fcc and hcp regions. At the right the lines in the fcc region line up whereas at the left the line in the hcp region is displaced from the fcc line as in Fig. 2(a). Moving toward the center of the herringbone corner, one finds an *extra row* in the hcp region in the bottom portion of the image. This extra row of atoms corresponds to a surface edge dislocation resulting from the different orientation of partial dislocations making up the two ridges which join to meet at the corner, as recently discussed by Chambliss *et. al*,[4] and shown clearly in Fig. 2(b).

Figure 3 shows the atomic structure of a 1nm triangular Fe island, which intersects multiple dislocation ridges. Fig. 3(a) shows the normal STM topograph, where maxima associated with individual Fe atoms are seen. The edge atoms surrounding the island have a lower contour; a lower edge charge density may result from the lower coordination of these atoms. Figure 3(b) shows an image of the same Fe island, enhanced by displaying the local curvature of the image. The complete structure of the island is observed overlaid

with an fcc(111) lattice net with a nearest neighbor distance of 0.288 nm. The agreement of the atomic positions with this lattice shows that the first layer of Fe is pseudomorphic with the Au(111) lattice with a nearest neighbor distance of 0.288 ±0.01 nm. The close-packed structure for Fe represents a metastable phase of room temperature Fe that does not occur naturally; normally the room temperature structure is the α-Fe bcc phase. By analyzing the rows of atoms in data at higher coverages where three layers are imaged, the stacking is determined to be fcc. The structure in Fig. 3(b) is expanded by 12% compared to the 0.257 nm in-plane nearest neighbor spacing of γ-Fe, which exists in bulk at higher temperature (910-1400 °C). Larger atom spacing favors ferromagnetism and increased magnetic moments suggesting that novel magnetic properties might be expected from such films of Fe on Au(111).

At a coverage of a few tenths monolayer, as shown in Fig. 4(a), triangular islands are observed which have their edges aligned with the close-packed $<1\bar{1}0>$ directions of the underlying fcc lattice, and typically alternate orientation in going along the herringbone from corner to corner. The Fe islands are a single monolayer high with an Fe-Au step height of 0.226 ± 0.01 nm (obtained in the voltage range of −1.0 to −1.5V). This step height is in between the Au-Au step height of 0.235 nm (taken for calibration and measured to a precision of ±0.005 nm) and the Fe-Fe step height of subsequent layers measured to be 0.209 ± 0.01 nm. The Fe-Fe step height is consistent with the (111) spacing of 0.210 nm for the fcc γ-Fe phase. Increasing the Fe exposure produces a coverage where the triangular Fe islands start to grow together, as shown in Fig. 4(b). At this coverage, 81% of the first layer is completed. Second layer nucleation is visible over an area corresponding to 4% of a monolayer. Further increase in Fe exposure shows good epitaxy for the first few layers, as seen by the very uniform first and second layer growth, which is flat on an atomic scale as seen in Fig. 4(c). At this 1.27 ML coverage, the growth front consists of the first layer at 92% completion and a substantial second layer growth at 32% completion; a small amount of 3rd layer growth, 3%, is also observed. The Au substrate

(indicated by the arrow) is seen through the voids in the first layer which comprise 8% of a monolayer.

At larger Fe film thicknesses, Fe prefers the bcc(110) crystal structure.[10,11] Evidence for this transition is shown in Fig. 4(d) at an Fe coverage of 3.2 ML where one observes a rectangular growth shape with an orientation along the $<11\bar{2}>_{fcc}$ directions. This suggests a transition to the bcc structure to release the strain in the Fe film. Coincident with this change in island shape, we observed a splitting in the diffraction streaks observed in RHEED experiments at the same Fe exposure. This coverage for the transition to bcc Fe is lower than observed in transmission electron microscopy studies (~7 ML);[10] however, in that investigation the Fe films were grown at elevated temperatures. The lattice mismatch between bcc Fe and the metastable fcc phases on the Au(111) surface can be seen by examining the bcc(110) and fcc(111) lattice nets.[10,11] While the $[100]_{bcc}$ lattice spacing of Fe is closely matched to the $[1\bar{1}0]_{fcc}$ Au lattice spacing (0.288 vs 0.287 nm), there is an 18.7% mismatch between the Fe $[01\bar{1}]_{bcc}$ lattice spacing of 0.406 nm and twice the Au $[11\bar{2}]_{fcc}$ lattice spacing of 0.499 nm. Such a large strain cannot be accommodated except for a few atomic layers, at which point the structure will revert to the normal room temperature bcc α-Fe phase.

An analysis of the layer occupation in the STM images yields a direct measure of the growth front during epitaxy, as shown in Fig. 5. A comparison of the growth fronts during the fcc and bcc growth is shown in Figs. 5(a)-(c). During the first few monolayers of fcc growth, the growth appears to be following a layer-by-layer mode with most of the growth confined in two layers, as seen in Fig. 5(a). The start of 4th layer growth with rectangular island shape is observed at 1.5 ML, as shown in Fig. 5(b). Subsequent growth in the bcc phase appears rougher with the growth front occupying 5-6 layers, as shown in Fig. 5(c). Note that the growth is still in layers which are atomically flat with terraces of order 10 nm; this is distinctly different than Volmer-Weber type growth, observed for example, with Fe on GaAs(110).[12]

In summary, we have shown the microscopic aspects of the growth of Fe on the Au(111) surface. Nucleation of Fe occurs at the corners of the Au(111) herringbone reconstruction with triangular growth shapes observed for the first layer islands. Atomic resolution measurements show pseudomorphic growth with a nearest neighbor in-plane lattice constant of 0.288 ± 0.01 nm and an Fe-Fe (111) step height of 0.209 ± 0.01 nm. The growth of the first few layers proceeds in a near layer-by-layer growth mode with a transition at 4 layers to rectangular shaped islands. The number of layers in the growth front increases with thickness. The STM data provide a precise determination of the details of the growth and a direct real space image of the growth front during epitaxy.

This work was supported in part by the Office of Naval Research.

References

1. For a review of thin film magnetism see L. M. Falicov, D. T. Pierce, S. D. Bader, R. Gronsky, K. B. Hathaway, H. J. Hopster, D. N. Lambeth, S. S. P. Parkin, G. Prinz, M. Salamon, I. K. Schuller, and R. H. Victora, J. Mater. Res. **5**, 1299 (1990).

2. A. S. Arrott, B. Heinrich, C. Liu, and S. T. Purcell, in *Thin Film Growth Techniques for Low-Dimensional Structures*, edited by R. F. C. Farrow, S. S. P. Parkin, P. J. Dobson, J. H. Neave, and A. S. Arrott (Plenum, New York, 1987), p. 287.

3. D. D. Chambliss and R. J. Wilson, J. Vac. Sci. Technol. B **9**, 928 (1991).

4. D. D. Chambliss, R. J. Wilson, and S. Chiang, Phys. Rev. Lett. **66**, 1721 (1991).

5. During the preparation of this manuscript, we learned of an STM study of Fe/Au(111) done independently by B. Voiglander, G. Meyer, and N. Amer (to be published).

6. J. H. van der Merwe and E. Bauer, Phys. Rev. B **39**, 3630 (1989).

7. P. I. Cohen, G. S. Petrich, P. R. Pukite, G. J. Whaley, and A. S. Arrott, Surf. Sci. **216**, 222 (1989).

8. J. V. Barth, H. Brune, G. Ertl, and R. J. Behm, Phys. Rev. B **42**, 9307 (1990).

9. J. Tersoff and D. R. Hamann, Phys. Rev. B **31**, 805 (1985).

10. G. Honjo, K. Takayanagi, K. Kobayashi, and K. Yagi, J. of Cryst. Growth **42**, 98 (1977).

11. E. Bauer and J. H. van der Merwe, Phys. Rev. B **33**, 3657 (1986).

12. R. A. Dragoset, P. N. First, J. A. Stroscio, D. T. Pierce, and R. J. Celotta, Materials Research Society Symposium Proceedings, Vol. 151, edited by B. T. Jonker, J. P. Heremans, and E. E. Marinero, (1989) p. 193; P. N. First, J. A. Stroscio, R. A. Dragoset, D. T. Pierce, and R. J. Celotta, Phys. Rev. Lett. **63**, 1416 (1989).

Figure Captions

Figure 1: STM images of 0.1 ML of Fe on Au(111). The grey scale cycles twice through the image to enhance contrast. (a) 80 x 56 nm image. (b) 29 x 29 nm image. The tunneling current was 0.5 nA and the sample bias was −1.0 and −1.5V for (a) and (b) respectively.

Figure 2: STM images of the clean Au(111) surface showing a close-up of the bulged herringbone corner. (a) 11 x 7 nm image showing the transition between fcc and hcp stacking. The average corrugation is 3 pm obtained at a tunneling current of 0.5 nA and sample bias of -0.9V. The image is shown without any filtering of the data. (b) A zoomed-in portion of the image in (a), 6.6 x 5.2 nm. The white lines align the $[0\bar{1}1]$ atomic rows across the herringbone corner with one extra column appearing in the hcp region indicated by the arrow.

Figure 3: STM image of a single monolayer high Fe island on the Au(111) surface. (a) STM topograph displayed as a 3-D rendered solid obtained at a tunneling current of 0.5 nA and sample bias of −0.2V. (b) Same image as (a) but with grey scale keyed to the negative of the surface curvature. The fcc(111) lattice net is shown overlaid on the image with a nearest neighbor lattice spacing of 0.288 nm.

Figure 4: STM images at various stages of growth of Fe on the Au(111) surface. (a) 115 x 115 nm image at 0.5 ML Fe coverage. (b) 115 x 115 nm image at 0.85 ML Fe coverage. (c) 58 x 58 nm image at 1.3 ML Fe coverage. (d) 100 x 100 nm image of 3.2 ML Fe coverage.

Figure 5: Fe layer occupation showing the growth front statistics at Fe coverages of (a)1.3 ML, (b) 1.5 ML, and (c) 3.2 ML. STM images, 50 x 50 nm, corresponding to these statistics are shown in insets.

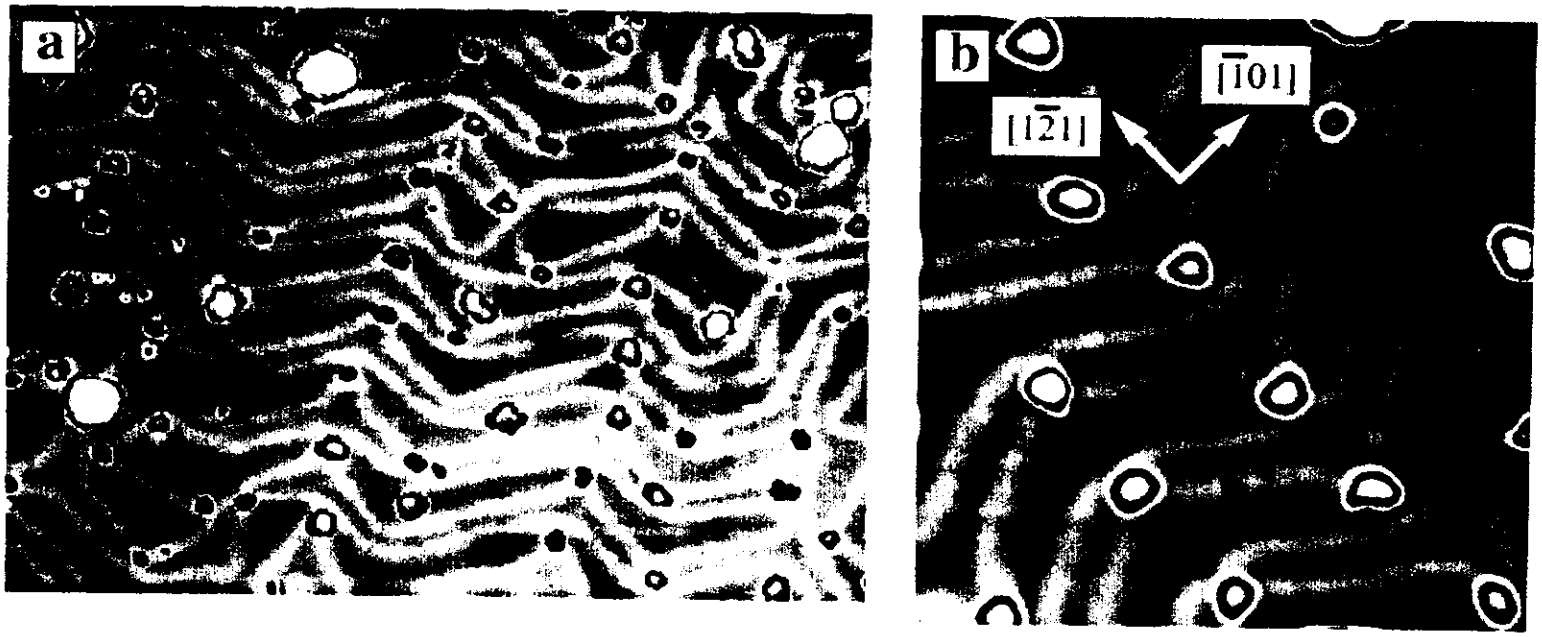

Fig. 1

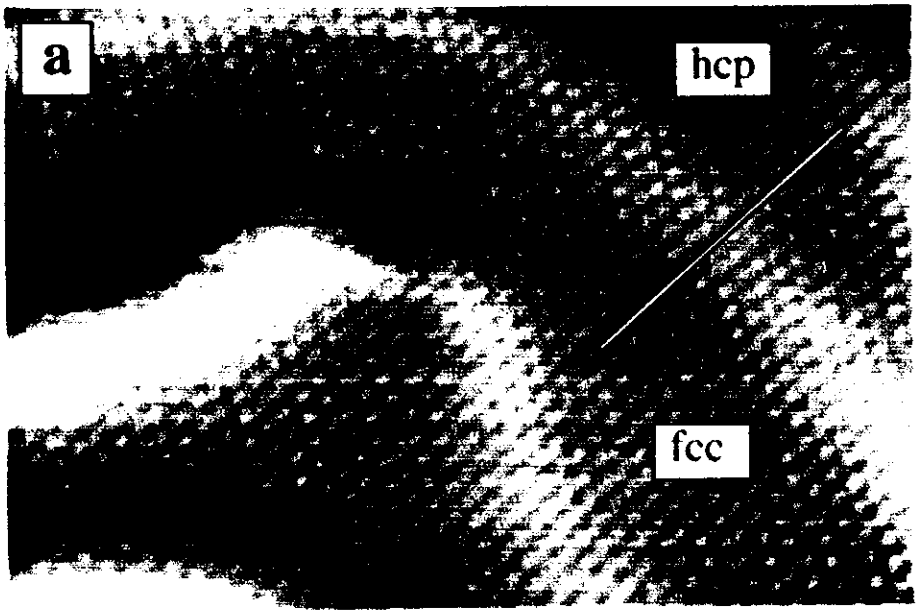

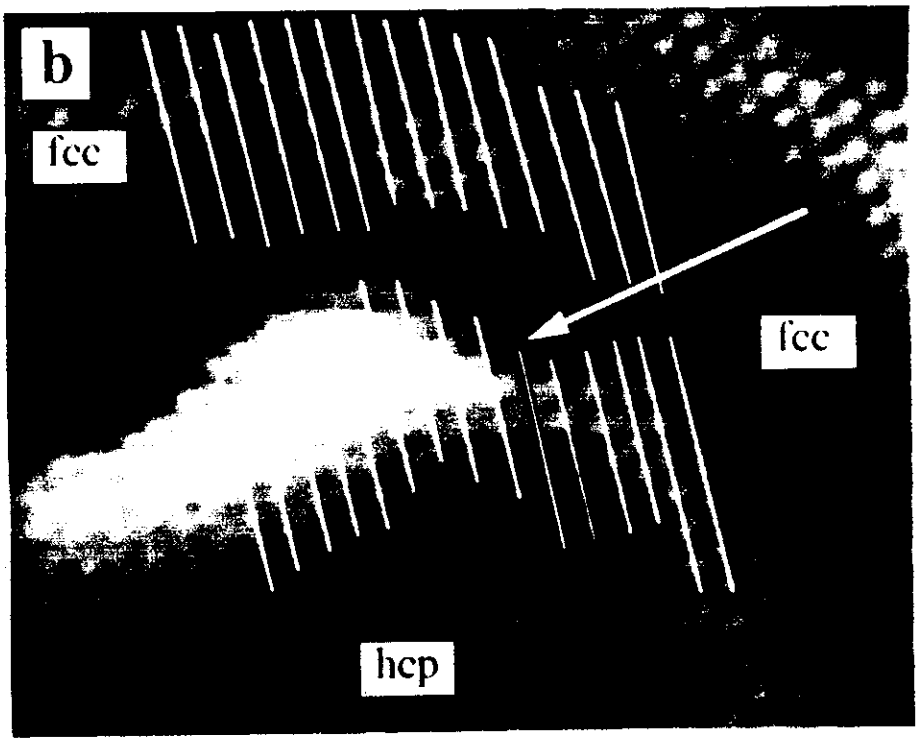

Fig. 7

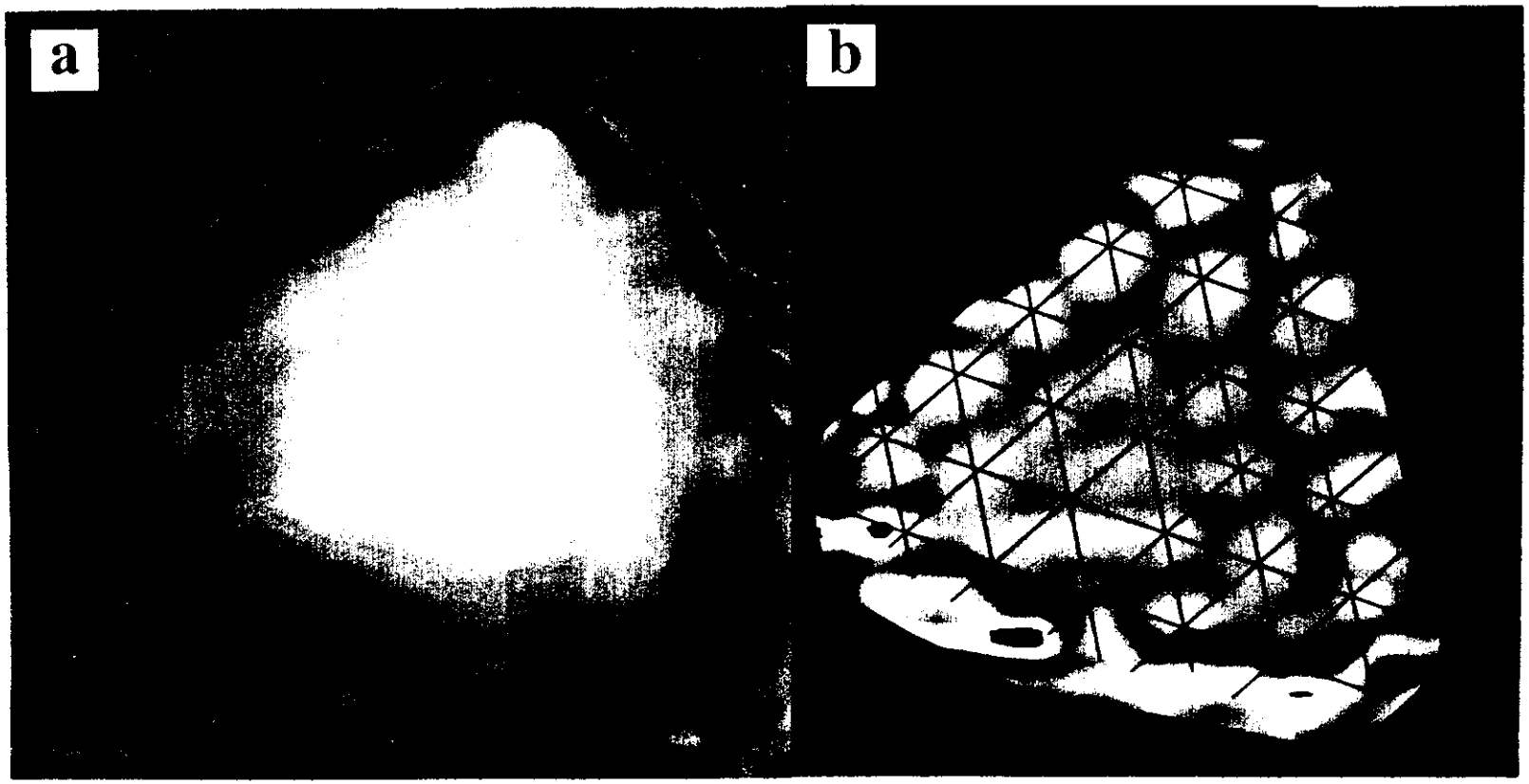

Fig 3

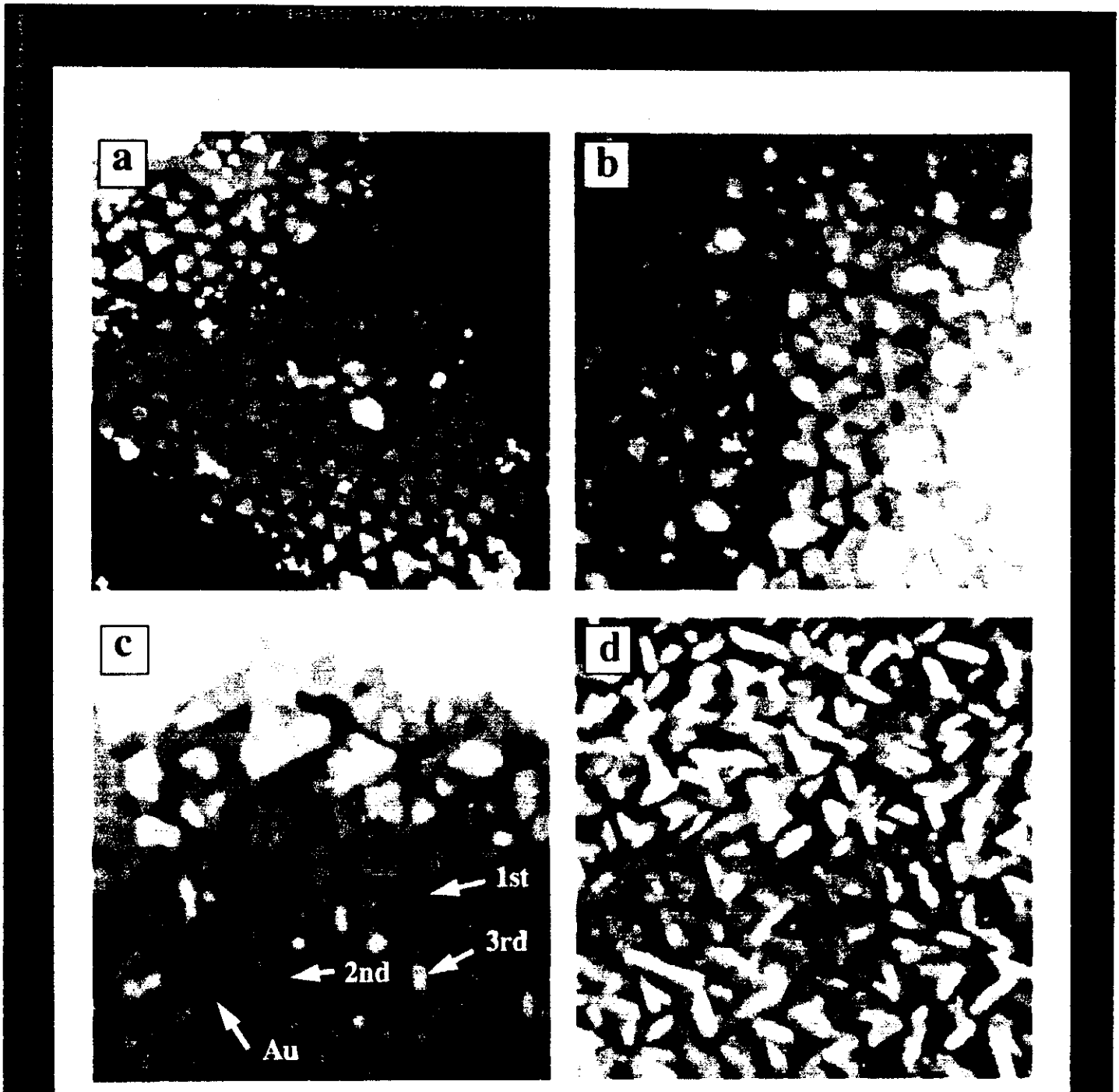

Fig. 4

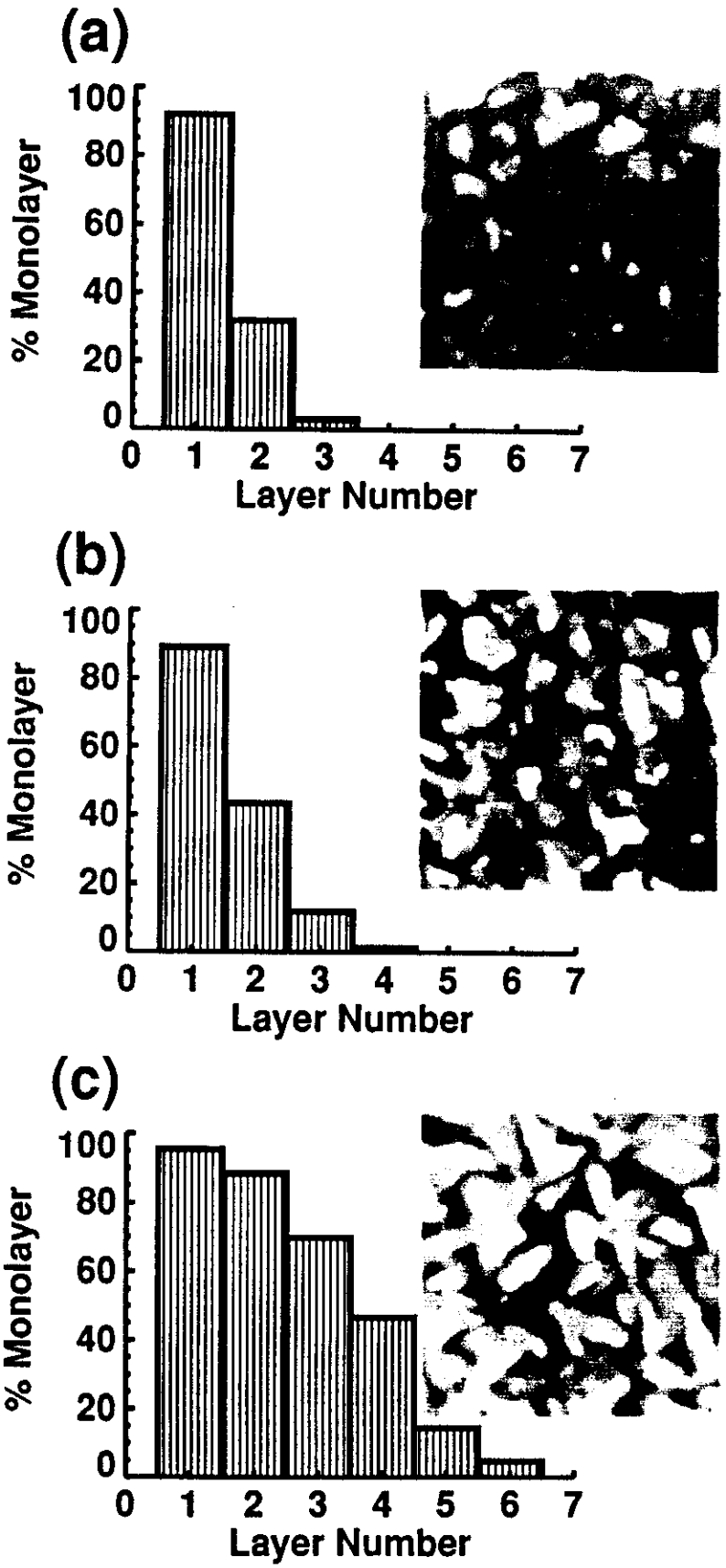
(a)
% Monolayer
100
80
60
40
20
0
0 1 2 3 4 5 6 7
Layer Number
(b)
% Monolayer
100
80
60
40
20
0
0 1 2 3 4 5 6 7
Layer Number
(c)
% Monolayer
100
80
60
40
20
0
0 1 2 3 4 5 6 7
Layer Number

Fig 5